Since January 2020 Elsevier has created a COVID-19 resource centre with free information in English and Mandarin on the novel coronavirus COVID-19. The COVID-19 resource centre is hosted on Elsevier Connect, the company's public news and information website.

Journal of Inorganic Biochemistry 234 (2022) 111886

Contents lists available at ScienceDirect

Journal of Inorganic Biochemistry

journal homepage: www.elsevier.com/locate/jinorgbio

Surface cysteines could protect the SARS-CoV-2 main protease from oxidative damage

Raheleh Ravanfar, Yuling Sheng, Mona Shahgholi, Brett Lomenick, Jeff Jones, Tsui-Fen Chou, Harry B. Gray *, Jay R. Winkler *

Beckman Institute, California Institute of Technology, 1200 East California Boulevard, Pasadena, CA 91125, USA

ARTICLE INFO

Keywords:
SARS-CoV-2 main protease
Reactive oxygen species
Cysteine

ABSTRACT

The SARS-CoV-2 main protease (M^{pro}) is responsible for cleaving twelve nonstructural proteins from the viral polyprotein. M^{pro}, a cysteine protease, is characterized by a large number of noncatalytic cysteine (Cys) residues, none involved in disulfide bonds. In the absence of a tertiary-structure stabilizing role for these residues, a possible alternative is that they are involved in redox processes. We report experimental work in support of a proposal that surface cysteines on M^{pro} can protect the active-site Cys145 from oxidation by reactive oxygen species (ROS). In investigations of enzyme kinetics, we found that mutating three surface cysteines to serines did not greatly affect activity, which in turn indicates that these cysteines could protect Cys145 from oxidative damage.

1. Introduction

The polycistronic replicase gene of SARS-CoV-2 encodes a large polyprotein that is cleaved into 15 nonstructural proteins by two cysteine proteases: a papain-like protease cleaves the first 3 proteins from the polypeptide (PL^{pro}); and the remaining 12 proteins are released by a 3-chymotrypsin-like protease ($3CL^{pro}$), often referred to as the main protease (M^{pro}) [1–3]. Owing to its critical role in the production of viral proteins, M^{pro} is a target for antiviral drug therapies [4–6]. Indeed, the antiviral drug PAXLOVID, which has received emergency use authorization for Covid-19 treatment, is an M^{pro} inhibitor. The active form of M^{pro} is a homodimer of two 306-residue polypeptides arranged in perpendicular orientation (Fig. 1) [7].

M^{pro} is unusually rich in cysteine residues [6,8]. Each monomer contains a His41-Cys145 dyad in the active site along with 11 additional Cys residues, none of which is involved in a cystine dimer. The M^{pro} Cys content (3.92% of residues) is three times greater than that of the average protein in the Uniprot database (1.3%). As of February 2, 2022, more than 7.1 million complete M^{pro} sequences from throughout the world had been deposited in the GISAID database. Among this total are 5884 unique M^{pro} sequences that include over 11,000 variations from the consensus sequence. Mutations in M^{pro} Cys residues were less common than average, occurring 171 times, with Cys156 (40 mutations) and Cys160 (39 mutations) being the most variable sites. Seven of the Cys residues are buried inside the protein, but five have moderate sidechain solvent accessibilities (>10% side chain exposure to solvent, Table 1). Thiols exposed on protein surfaces interact directly with the intracellular environment and are important components of the redox proteome [9]. As a component of the human innate immune response is the production of reactive oxygen species (ROS) [10–12], one role for the noncatalytic M^{pro} Cys residues might be to protect the active site Cys145 by rapidly reducing these potentially disabling oxidants.

The M^{pro} surface Cys residues can provide useful protection to Cys145 only if their modification does not substantially reduce enzyme activity. A prior study demonstrated that Cys300Ser and Asp155Ala|Cys156Ser mutations had little impact on M^{pro} activity [13]. We have examined the enzymatic kinetics of wild-type M^{pro} and that of a triple mutant in which three of the most highly solvent-exposed Cys residues were replaced by serine (Cys85Ser|Cys156Ser|Cys300Ser). We found that the triple mutant maintained the homodimeric structure required for protease function and that its activity was only modestly reduced from that of the wild-type enzyme.

2. Results and discussion

The M^{pro} gene from SARS-CoV-2 strain was expressed in BL21 *Escherichia coli* with a C-terminal $(His)_6$-tag. We employed IAEDANS (5-((2-iodoacetyl)-amino)ethyl)amino)naphthalene-1-sulfonic acid) to

* Corresponding authors.
E-mail addresses: hbgray@caltech.edu (H.B. Gray), winklerj@caltech.edu (J.R. Winkler).

https://doi.org/10.1016/j.jinorgbio.2022.111886
Received 2 March 2022; Received in revised form 28 April 2022; Accepted 29 May 2022
Available online 2 June 2022

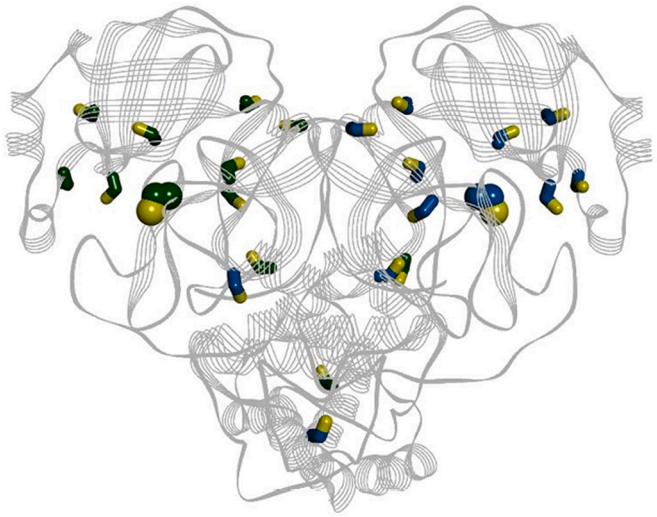

Fig. 1. Ribbon diagram based on the X-ray structure of the SARS-CoV-2 M^{pro} (PDB code 6Y2E) [2]. The C_α and C_β atoms of the 11 noncatalytic cysteine residues are shown as green and blue sticks in each monomer; the S_γ atoms rendered in yellow. The C_α, C_β, and S_γ atoms of the catalytic cysteine are shown as spheres in each monomer. (For interpretation of the references to colour in this figure legend, the reader is referred to the web version of this article.)

identify the most reactive M^{pro} surface Cys residues. UV/vis spectra of IAEDANS-labeled M^{pro} after 1, 2, 4, and 12 h (Fig. S3) confirmed IAEDANS conjugation to M^{pro} and the IAEDANS:M^{pro} ratio increased with reaction time. LC-MS measurements indicated that three to four molecules of IAEDANS attached to M^{pro} in 4–12 h (Fig. S4). MS/MS spectra of tryptic digests with 64.9% sequence coverage provided strong evidence that IAEDANS labeled Cys44 and Cys85 (Fig. S5). MS/MS results from chymotrypsin digests revealed C300 IAEDANS-labeling (and possibly partial labeling of Cys85, Cys117, and Cys145, Fig. S6). These results, in combination with sidechain solvent accessibility estimates from the crystal structure, suggested three candidates for mutation: Cys85, Cys156, and Cys300 (Table 1). Based on this information, we expressed and purified a $(His)_6$-tagged M^{pro} triple mutant (Cys85Ser|Cys156Ser|Cys300Ser) (Fig. S1b).

M^{pro} is catalytically active only as a homodimer: the N-terminal amine of one monomer hydrogen bonds to Glu166 in the other monomer, shaping the pocket of the substrate binding site [14]. We used native-gel electrophoresis to confirm that both the M^{pro} triple mutant and wild type are homogenous homodimers (Fig. 2a). We determined the oligomeric state of each enzyme in solution using combined size exclusion chromatography and multi-angle light scattering (SEC-MALS) [15]. Each protein migrated on an SEC column as a single monodispersed peak with a derived molar mass in good agreement with that expected for a dimer (wild type, $8.60 \times 10^4 \pm 3.2\%$; triple mutant $8.62 \times 10^4 \pm 3.7\%$) (Fig. 2b). No monomer was detected, indicating that the C-terminal $(His)_6$-tag did not interfere with M^{pro} dimerization. The far-UV CD spectra (Fig. 3) of the wild type and mutant enzymes exhibited peaks at 222 and 207 nm that are in good agreement with published spectra [16], and are consistent with a predominantly β-sheet/short α-helical fold, as found in the crystal structure [2]. Near-UV CD spectra report on the environments of phenylalanine (255–270 nm), tyrosine (275–282 nm), and tryptophan (290–305 nm) residues and provide insight to the overall tertiary structure of a protein [17]. Each Mpro monomer has 17 Phe, 11 Tyr, and 3 Trp residues. The near-UV CD spectra of wild-type and triple mutant M^{pro} are closely similar in the Phe and Tyr regions (250–282 nm), with a minor deviation in the Trp region. Thermal denaturation probed by 220 nm CD reveals that the triple mutant is only slightly less stable than the wild-type protein (denaturation midpoints: wild-type 57 °C; triple mutant, 52 °C, Fig. S12). Taken together, the data indicate that the overall protein structure is not substantially perturbed by mutation of the three surface Cys residues to Ser.

To evaluate the activities of wild type and triple mutant enzymes, we examined the kinetics of their reactions with a synthetic tetrapeptide containing two non-natural amino acids: Ac-Abu-Tle-Leu-Gln-AMC (Abu is L-2-aminobutyric acid; Tle is L-*tert*-leucine). The oligopeptide has a C-terminal amide link to a fluorescent dye (7-amino-4-methylcoumarin, AMC) [5]. Hydrolysis by SARS-CoV-2 M^{pro} between Gln and AMC released free coumarin and produced a substantial increase in 440-nm fluorescence intensity.

We tested the M^{pro} proteolytic activity of the wild type and triple mutant enzymes at pH 7.8 at substrate concentrations in the range 0–90 μM. We found that the reaction of substrate with triple mutant M^{pro} was measurably slower than that of the wild-type enzyme at all investigated substrate concentrations (Fig. S7, S8). The concentration of hydrolyzed product increased linearly with time during the first 20 min of reaction at room temperature (Fig. S10). Initial reaction velocities, scaled by enzyme concentration, were linear functions of substrate concentration (0–90 μM) without apparent saturation (Fig. 4). This observation indicates relatively weak binding of the substrate to M^{pro}, consistent with the previously reported Michaelis constant of 207 ± 12 μM [5]. Apparent second-order rate constants (k_{obsd}) determined from four replicates of the reaction of M^{pro} with the substrate are 79 ± 16 and 28 ± 8 M^{-1} s^{-1} (~22 °C) for wild type and triple mutant, respectively (Fig. 4, Fig. S11). For comparison, wild-type activity at 37 °C was reported to be 859 ± 57 M^{-1} s^{-1} [5]. The reduced activity of the triple mutant is likely attributable to the Cys85Ser mutation since individual replacements of Cys156 and Cys300 had negligible impact on activity [13]. Cys85 is positioned in a loop identified as the catalytic acid zone of trypsin-like proteases and its replacement with Ser could impart a modest perturbation of the catalytic active site [18,19].

Our finding that the activity of the triple mutant (Cys85Ser|Cys156Ser|Cys300Ser) was only reduced 2.8-fold from that of wild type is consistent with the proposal that M^{pro} surface cysteines could protect the active-site Cys145 from ROS-triggered oxidative damage.

3. Materials and methods

Detailed descriptions of materials and procedures used for the expression, purification, and characterization of wild-type and mutant M^{pro}, as well as measurements of reaction kinetics, are provided in Supplementary Data.

CRediT authorship contribution statement

Raheleh Ravanfar: Investigation, Methodology, Writing – original draft, Writing – review & editing. **Yuling Sheng:** Investigation. **Mona Shahgholi:** Investigation, Methodology, Writing – review & editing. **Brett Lomenick:** Investigation, Methodology, Formal analysis, Writing

Table 1
Percent solvent accessible surface areas of M^{pro} Cys residue sidechains.[a]

Cys16	Cys22	Cys38	Cys44	Cys85	Cys117	Cys128	Cys145	Cys156	Cys160	Cys265	Cys300
2.6	3.4	5.2	0.7	26.0	2.3	15.4	40.3	39.7	3.3	6.0	29.8

[a] Solvent accessible surface areas determined on the M^{pro} (PDB ID 6Y2E) structure using the Biovia Discovery Studio Visualizer package with a 1-Å probe radius and 960 grid points per atom.

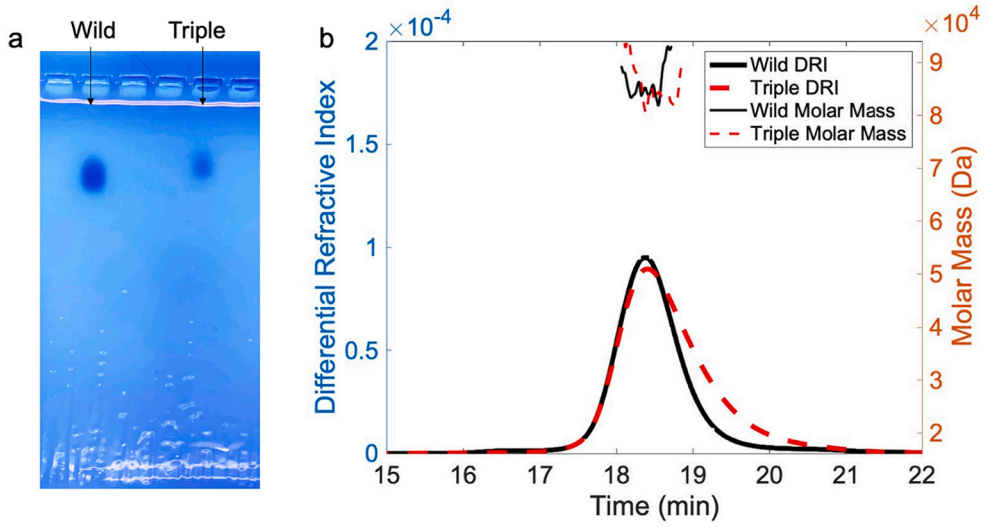

Fig. 2. a) Native gel electrophoresis shows only pure homodimers of wild type (left) and triple mutant M^{pro} (right). b) SEC-MALS analysis of wild type (black) and triple mutant (red) M^{pro}; the left ordinate (blue) indicates the differential refractive index from SEC; and the right ordinate (orange) shows the molar mass extracted from MALS. (For interpretation of the references to colour in this figure legend, the reader is referred to the web version of this article.)

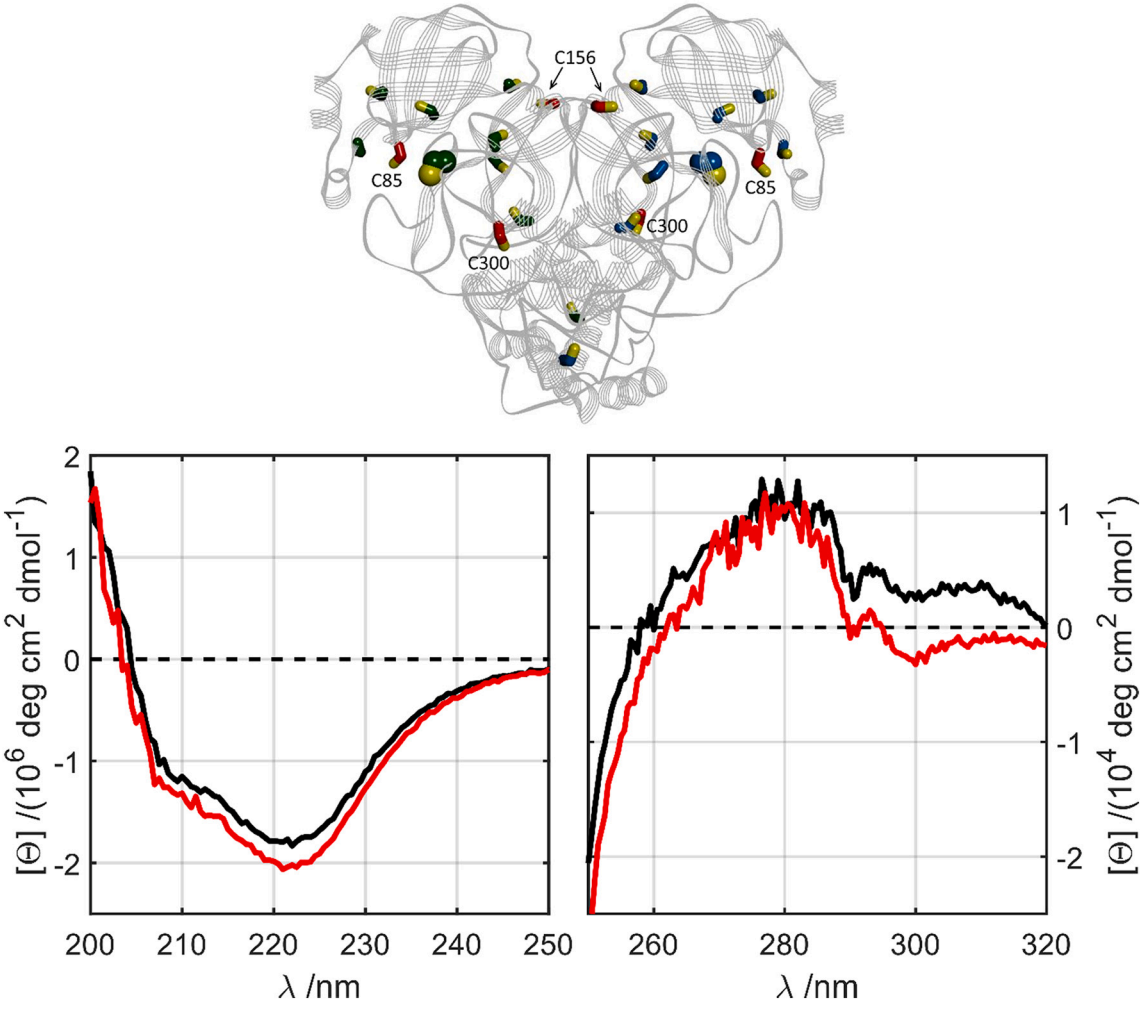

Fig. 3. (upper) Structural model of SARS-Cov-2 M^{pro} highlighting the mutation sites (Cys85, Cys156, and Cys300: C_α and C_β atoms in red). The Cys145 residues are shown as spheres in each monomer. (lower) Far-UV (left) and near-UV (right) CD spectra of wild type (black) and triple mutant (red) M^{pro}. (For interpretation of the references to colour in this figure legend, the reader is referred to the web version of this article.)

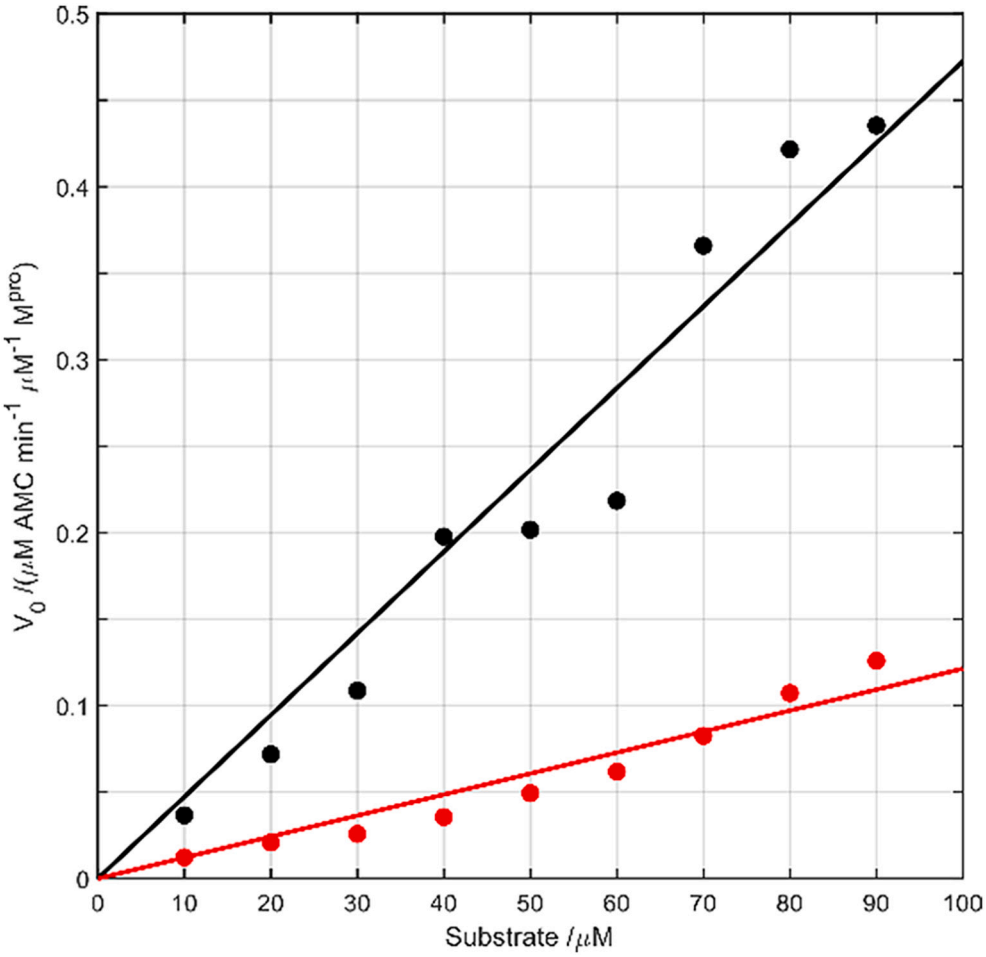

Fig. 4. Representative plots of M^{pro} reaction velocities at pH 7.8 as functions of substrate concentration: wild type (black, solid line corresponds to an observed rate constant of 79 M^{-1} s^{-1}); (b) triple mutant (red, k_{obsd} = 20 M^{-1} s^{-1}). (For interpretation of the references to colour in this figure legend, the reader is referred to the web version of this article.)

– review & editing. **Jeff Jones:** Investigation, Methodology, Formal analysis, Writing – review & editing. **Tsui-Fen Chou:** Writing – review & editing, Methodology. **Harry B. Gray:** Funding acquisition, Project administration, Writing – review & editing. **Jay R. Winkler:** Conceptualization, Funding acquisition, Project administration, Writing – review & editing.

Declaration of Competing Interest

The authors declare that they have no known competing financial interests or personal relationships that could have appeared to influence the work reported in this paper.

Acknowledgements

We thank Dr. Jennifer Keeffe for assistance with SEC-MALS. Experimental work was performed in the Caltech Mass Spectrometry Laboratory in the Division of Chemistry and Chemical Engineering; and the Beckman Institute Laser Resource Center and Proteome Exploration Laboratory supported by the Arnold and Mabel Beckman Foundation. The work was supported by the National Institute of Diabetes and Digestive and Kidney Diseases of the National Institutes of Health under award number R01DK019038. The content is solely the responsibility of the authors and does not necessarily represent the official views of the National Institutes of Health.

Appendix A. Supplementary data

Supplementary data to this article can be found online at https://doi.org/10.1016/j.jinorgbio.2022.111886.

References

[1] A.R. Fehr, S. Perlman, in: H.J. Maier, E. Bickerton, P. Britton (Eds.), Coronaviruses: Methods and Protocols, Springer, New York, New York, NY, 2015, pp. 1–23, https://doi.org/10.1007/978-1-4939-2438-7_1.

[2] L. Zhang, D. Lin, X. Sun, U. Curth, C. Drosten, L. Sauerhering, S. Becker, K. Rox, R. Hilgenfeld, Crystal structure of SARS-CoV-2 main protease provides a basis for design of improved α-ketoamide inhibitors, Science 368 (6489) (2020) 409–412, https://doi.org/10.1126/science.abb3405.

[3] L. Zhu, S. George, M.F. Schmidt, S.I. Al-Gharabli, J. Rademann, R. Hilgenfeld, Peptide aldehyde inhibitors challenge the substrate specificity of the SARS-coronavirus main protease, Antivir. Res. 92 (2) (2011) 204–212, https://doi.org/10.1016/j.antiviral.2011.08.001.

[4] J. Qiao, Y.-S. Li, R. Zeng, F.-L. Liu, R.-H. Luo, C. Huang, Y.-F. Wang, J. Zhang, B. Quan, C. Shen, X. Mao, X. Liu, W. Sun, W. Yang, X. Ni, K. Wang, L. Xu, Z.-L. Duan, Q.-C. Zou, H.-L. Zhang, W. Qu, Y.-H.-P. Long, M.-H. Li, R.-C. Yang, X. Liu, J. You, Y. Zhou, R. Yao, W.-P. Li, J.-M. Liu, P. Chen, Y. Liu, G.-F. Lin, X. Yang, J. Zou, L. Li, Y. Hu, G.-W. Lu, W.-M. Li, Y.-Q. Wei, Y.-T. Zheng, J. Lei, S. Yang, SARS-CoV-2 M^{pro} inhibitors with antiviral activity in a transgenic mouse model, Science 371 (6536) (2021) 1374–1378, https://doi.org/10.1126/science.abf1611.

[5] W. Rut, K. Groborz, L. Zhang, X. Sun, M. Zmudzinski, B. Pawlik, X. Wang, D. Jochmans, J. Neyts, W. Młynarski, R. Hilgenfeld, M. Drag, SARS-CoV-2 Mpro inhibitors and activity-based probes for patient-sample imaging, Nat. Chem. Biol. 17 (2) (2021) 222–228, https://doi.org/10.1038/s41589-020-00689-z.

[6] J.J. Kozak, H.B. Gray, R.A. Garza-López, Structural stability of the SARS-CoV-2 main protease: can metal ions affect function? J. Inorg. Biochem. 211 (2020), 111179 https://doi.org/10.1016/j.jinorgbio.2020.111179.

[7] L. Silvestrini, N. Belhaj, L. Comez, Y. Gerelli, A. Lauria, V. Libera, P. Mariani, P. Marzullo, M.G. Ortore, A., Palumbo Piccionello, the dimer-monomer equilibrium of SARS-CoV-2 main protease is affected by small molecule inhibitors, Sci. Rep. 11 (1) (2021) 1–16, https://doi.org/10.1038/s41598-021-88630-9.
[8] D.W. Kneller, G. Phillips, K.L. Weiss, S. Pant, Q. Zhang, H.M. O'Neill, L. Coates, A. Kovalevsky, Unusual zwitterionic catalytic site of SARS–CoV-2 main protease revealed by neutron crystallography, J. Biol. Chem. 295 (50) (2020) 17365–17373, https://doi.org/10.1074/jbc.AC120.016154.
[9] Y.-M. Go, D.P. Jones, The redox proteome, J. Biol. Chem. 288 (37) (2013) 26512–26520, https://doi.org/10.1074/jbc.R113.464131.
[10] C.N. Paiva, M.T. Bozza, Are reactive oxygen species always detrimental to pathogens? Antioxid. Redox Signal. 20 (6) (2014) 1000–1037, https://doi.org/10.1089/ars.2013.5447.
[11] V. Naumenko, M. Turk, C.N. Jenne, S.-J. Kim, Neutrophils in viral infection, Cell Tissue Res. 371 (3) (2018) 505–516, https://doi.org/10.1007/s00441-017-2763-0.
[12] E.E. To, R. Vlahos, R. Luong, M.L. Halls, P.C. Reading, P.T. King, C. Chan, G. R. Drummond, C.G. Sobey, B.R.S. Broughton, M.R. Starkey, R. van der Sluis, S. R. Lewin, S. Bozinovski, L.A.J. O'Neill, T. Quach, C.J.H. Porter, D.A. Brooks, J. J. O'Leary, S. Selemidis, Endosomal NOX2 oxidase exacerbates virus pathogenicity and is a target for antiviral therapy, Nat. Commun. 8 (1) (2017) 69, https://doi.org/10.1038/s41467-017-00057-x.
[13] X. Tao, L. Zhang, L. Du, R. Liao, H. Cai, K. Lu, Z. Zhao, Y. Xie, P.-H. Wang, J.-A. Pan, Y. Zhang, G. Li, J. Dai, Z.-W. Mao, W. Xia, Allosteric inhibition of SARS-CoV-2 3CL protease by colloidal bismuth subcitrate, Chem. Sci. 12 (42) (2021) 14098–14102, https://doi.org/10.1039/D1SC03526F.
[14] K. Anand, G.J. Palm, J.R. Mesters, S.G. Siddell, J. Ziebuhr, R. Hilgenfeld, Structure of coronavirus main proteinase reveals combination of a chymotrypsin fold with an extra α-helical domain, EMBO J. 21 (13) (2002) 3213–3224, https://doi.org/10.1093/emboj/cdf327.
[15] P.J. Wyatt, Light scattering and the absolute characterization of macromolecules, Anal. Chim. Acta 272 (1) (1993) 1–40, https://doi.org/10.1016/0003-2670(93)80373-S.
[16] J.C. Ferreira, W.M. Rabeh, Biochemical and biophysical characterization of the main protease, 3-chymotrypsin-like protease (3CLpro) from the novel coronavirus SARS-CoV 2, Sci. Rep. 10 (1) (2020) 22200, https://doi.org/10.1038/s41598-020-79357-0.
[17] M.S. Kelly, C.N. Price, The use of circular dichroism in the investigation of protein structure and function, Curr. Protein Pept. Sci. 1 (4) (2000) 349–384, https://doi.org/10.2174/1389203003381315.
[18] A.I. Denesyuk, E.A. Permyakov, M.S. Johnson, S.E. Permyakov, K. Denessiouk, V. N. Uversky, Structural and functional significance of the amino acid differences Val35Thr, Ser46Ala, Asn65Ser, and Ala94Ser in 3C-like proteinases from SARS-CoV-2 and SARS-CoV, Int. J. Biol. Macromol. 193 (2021) 2113–2120, https://doi.org/10.1016/j.ijbiomac.2021.11.043.
[19] A.I. Denesyuk, S.E. Permyakov, M.S. Johnson, E.A. Permyakov, V.N. Uversky, K. Denessiouk, Structural leitmotif and functional variations of the structural catalytic core in (chymo)trypsin-like serine/cysteine fold proteinases, Int. J. Biol. Macromol. 179 (2021) 601–609, https://doi.org/10.1016/j.ijbiomac.2021.03.042.